International Scholarly Research Network
ISRN Nanotechnology
Volume 2012, Article ID 604241, 11 pages
doi:10.5402/2012/604241

Research Article

An Overview on Nanocrystalline $ZnFe_2O_4$, $MnFe_2O_4$, and $CoFe_2O_4$ Synthesized by a Thermal Treatment Method

Mahmoud Goodarz Naseri,[1,2] Elias B. Saion,[1] and Ahmad Kamali[1]

[1] *Department of Physics, Universiti Putra Malaysia, 43400 UPM Serdang, Selangor, Malaysia*
[2] *Department of Physics, Faculty of Science, Malayer University, Malayer, Iran*

Correspondence should be addressed to Mahmoud Goodarz Naseri, mahmoud.naseri55@gmail.com

Received 5 April 2012; Accepted 6 May 2012

Academic Editors: G. H. Lee, G. Li, V. Popok, and J. J. Suñol

This study reports the simple synthesis of MFe_2O_4 (where M = Zn, Mn, and Co) nanoparticles by a thermal treatment method, followed by calcination at various temperatures from 723 to 873 K. Poly(vinyl pyrrolidone) (PVP) was used as a capping agent to stabilize the particles and prevent them from agglomeration. The characterization studies were conducted by X-ray diffraction (XRD) and transmission electron microscopy (TEM). The average particle sizes were obtained by TEM images, which were in good agreement with the XRD results. Fourier transform infrared spectroscopy (FT-IR) confirmed the presence of metal oxide bands for all the calcined samples. Magnetic properties were demonstrated by a vibrating sample magnetometer (VSM), which displayed that the calcined samples exhibited superparamagnetic and ferromagnetic behaviors.

1. Introduction

Nanoscience and nanotechnology are involved in the manipulation of materials and the creation of structures and systems at the nanometer scale. As a result, nanomaterials have attracted much attention because of their surface effect (large surface-to-volume ratio) and quantum confinement effects (size-dependent properties). These factors affect their physical and chemical properties, which differ from the properties of their molecular and bulk counterparts. Nanoparticles with zero-dimensional nanostructures are generally classified according to their compositions, that is, metal oxides, noble metals, transition metals, magnetic metals, and semiconductor nanomaterials or quantum dots. Like all nanostructures, magnetic metals nanoparticles are dependent on their size and shape. Currently, magnetic oxide nanoparticles are attracting significant interest due to their extensive applications, ranging from fundamental research to industrial use. Spinel nanocrystals are regarded as two of the most important inorganic nanomaterials because of their electronic, optical, electrical, magnetic, and catalytic properties. Spinel has the structure AB_2O_4 in which A and B display tetrahedral and octahedral cation sites, respectively, and O indicates the oxygen anion site. Metal spinel ferrite nanoparticles have the general molecular formula MFe_2O_4 (e.g., M = Ni, Zn, Mn, Co, or Mg), and they have a face-centered-cubic (fcc) close packing structure. Among the spinel ferrites compounds, zinc ferrite, manganese ferrite, and nickel ferrite have been studied extensively due to their different structures composed of inverse, normal, and mixed spinel structures, respectively, and their high electromagnetic performance, excellent chemical stability, mechanical hardness, low coercivity, and moderate saturation magnetization, which make it a good contender for the application as soft magnets and low-loss materials at high frequencies [1–3]. These properties are dependent on the chemical composition and microstructural characteristics in which the particle size and shape might be controlled in the fabrication processes. In order to achieve materials that have the desired physical and chemical properties, the preparation of spinel ferrites nanocrystals through different routes has become an essential focus of the related research and development activities. Various fabrication methods to prepare spinel ferrites nanocrystals have been reported, for example, sol-gel methods [4], the ball-milling technique [5], coprecipitation [6], polymeric-assisted route [7], the hydrothermal method [8], the reverse micelles process [9], and the microemulsion method [10]. Various precipitation agents have been used to

produce specific size and shape spinel ferrites nanocrystals, for example, metal hydroxide in the coprecipitation method, surfactant and ammonia in the reverse micelles process and various microemulsion methods, and organic matrices in the sol-gel method. Most of these methods have achieved particles of the required sizes and shapes, but they are difficult to employ on a large scale because of their expensive and complicated procedures, high reaction temperatures, long reaction times, toxic reagents and by-products, and their potential harm to the environment. In the present study, spinel ferrites nanocrystals with different structures were prepared from an aqueous solution containing metal nitrates, poly(vinyl pyrrolidone), and deionized water using a low temperature thermal treatment method, followed by grinding and calcination.

2. Experimental

2.1. Materials. In this study, metal nitrate reagents, poly(vinyl pyrrolidone) (PVP), and deionized water were used as precursors. In addition, a capping agent to control the agglomeration of the particles and a solvent were used. Iron nitrate, $Fe(NO_3)_3 \cdot 9H_2O$, zinc nitrate, $Zn(NO_3)_2 \cdot 6H_2O$, manganese nitrate, $Mn(NO_3)_2 \cdot 6H_2O$, and nickel nitrate, $Co(NO_3)_2 \cdot 6H_2O$, were purchased from Acros Organics with a purity exceeding 99%. PVP (MW = 29000) was purchased from Sigma Aldrich and was used without further purification. An aqueous solution of PVP was prepared by dissolving of polymer in 100 mL of deionized water at 363 K, before mixing 0.2 mmol iron nitrate and 0.1 mmol metal nitrate (Fe : M = 2 : 1) into the polymer solution and constantly stirring for 2 h using a magnetic stirrer until a colorless, transparent solution was obtained. A glass electrode was used to determine the pH of the solution, which ranged from 1 to 2. The mixed solution was poured into a glass Petri dish and heated at 353 K in an oven for 24 h to evaporate the water. The dried, orange, solid zinc ferrite that remained was crushed and ground in a mortar to form powder. The calcinations of the powders were conducted at 723, 773, 823, and 873 K for 3 h for the decomposition of organic compounds and the crystallization of the nanocrystals. (Note that 3 h was the minimum time that allowed the crystallization to be completed.) The processing steps are employed separately for the synthesis of each ferrite nanoparticles.

2.2. Characterization. The structure of the $ZnFe_2O_4$, $MnFe_2O_4$, and $CoFe_2O_4$ nanoparticles was characterized by the XRD technique using a Shimadzu diffract meter model XRD 6000 employing CuK_α (0.154 nm) radiation to generate diffraction patterns from powder crystalline samples at ambient temperature in a 2θ range of 10° to 70°. The microstructure and particle size of the nanocrystals were determined from transmission electron microscopy (TEM) images that were obtained by using a JEOL 2010F UHR version electron microscope at an accelerating voltage of 200 kV. FT-IR spectra were recorded using a PerkinElmer FT-IR model 1650 spectrometer. Before recording spectra, the samples were placed on a Universal ATR Sampling Accessory (diamond coated with CsI) and pressed, and then the spectra were recorded. Magnetization measurements were conducted using a vibrating sample magnetometer (VSM) (Lake Shore 4700) at room temperature with maximum magnetic field of 15 kOe.

3. Results and Discussion

3.1. Mechanism of Interaction of PVP and Metal Ions in Synthesize of Metal Ferrite Nanoparticles. Interactions between the PVP capping agent [11] and metal ions are shown schematically in Figure 1. We have shown the metal (II) (e.g., Zn, Mn, and Co) and iron (III) ions which are bound by the strong ionic bonds between the metallic ions and the amide group in a polymeric chain. PVP acts as a stabilizer for dissolved metallic salts through steric and electrostatic stabilization of the amide groups of the pyrrolidine rings and the methylene groups. Initially, the PVP stabilizer may decompose to as limited extent, thereby producing shorter polymer chains that are capped when they are adsorbed onto the surfaces of metallic ions [12]. The metallic ions, which are well dispersed in the cavities and networks, are created as a result of the shorter polymer chains. These mechanisms continue until they are terminated by the drying step. The influence of PVP is not restricted only to the solution and the drying step; PVP also affects the formation of the nuclei (i.e., nucleation) of the metal ferrite nanoparticles in the calcination step. In this step, the small nanoparticles with high surface energy levels would become larger via the Ostwald ripening process [13] without the presence of PVP, disrupts steric hindrance, thereby preventing their aggregation. Steric hindrance is a phenomenon that is attributed to large molecular weight (>10,000) and the repulsive forces acting among the polyvinyl groups [14, 15]. These interactions are similar to the stabilization of metallic nanoparticles, that is, silver and gold [16, 17].

3.2. Phase Composition and Morphology of Precursors and Metal Ferrite Nanoparticles. XRD and FT-IR were used to characterize the precursors and ferrite nanoparticles calcined at 723, 773, 823, and 873 K. The XRD diffraction patterns of the precursor and metal ferrite nanoparticles are shown in Figure 2. A broad peak occurred for all samples in the precursor, which does not have sharp diffraction patterns and is still amorphous. The calcined patterns show the reflection planes (111), (220), (311), (222), (400), (331), (422), (511), and (440), which confirm the presence of single-phase in $ZnFe_2O_4$, $MnFe_2O_4$, and $CoFe_2O_4$ with a face-centered cubic structure [18–20]. Except for the impure phases of α-Fe_2O_3 (for all the metal ferrite nanoparticles shown in Figures 2(a), 2(b), and 2(c)) and ZnO (for the zinc ferrite nanoparticles shown in Figure 2(a)), which occur naturally as hematite and zincite, respectively [18–21], the remaining peaks correspond to the standard pattern of $ZnFe_2O_4$ (cubic, space group: Fd3m, $Z = 8$; ICDD PDF: 22–1012), $MnFe_2O_4$ (cubic, space group: Fd3m, $Z = 8$; ICDD

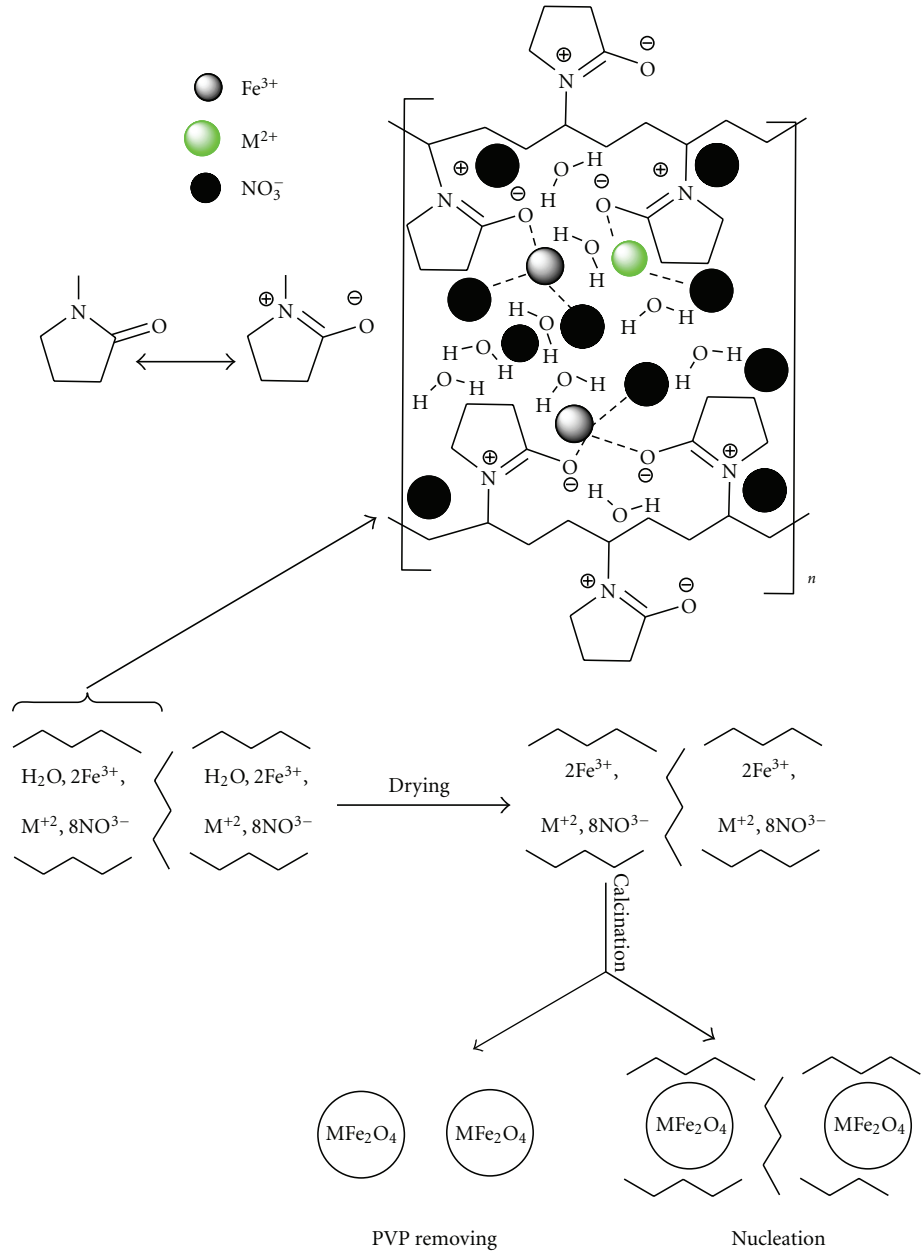

Figure 1: The proposed mechanism of interactions between PVP and metal ions in the formation of the metal ferrites nanoparticles.

PDF: 73–1964), and $CoFe_2O_4$ (cubic, space group: Fd3m, Z = 8; ICDD PDF: 22–1086) [18–20].

The results obtained from XRD were analyzed using the Chekcell program, which calculated lattice parameters of the samples calcined at 723, 773, 823, and 873 K (Table 1). XRD results were analyzed by the Scherer formula:

$$D = \frac{0.9\lambda}{\beta \cos \theta}, \quad (1)$$

where D is the crystallite size (nm), β is the full width of the diffraction line at half the maximum intensity measured in radians, λ is X-ray wavelength, and θ is the Bragg angle [22]. This formula was used to estimate the average particle sizes, which ranged in Table 1.

Figure 3 shows the FT-IR spectrum of the precursor and calcined samples in the wave-number range between 280 and 4000 cm^{-1}. The IR spectra of all calcined samples show the two principle absorption bands in the range of 300–600 cm^{-1}. These two vibration bands Fe↔O and M↔O are corresponded to the intrinsic lattice vibrations of octahedral and tetrahedral coordination compounds in the spinel structure, respectively [23]. The bands with peaks around 670 and 850 cm^{-1} were assigned to the formation vibration of C–N=O bending and the C–C ring. The bands in the range of 1200 to 1250 cm^{-1} were associated with C–N stretching vibration, and the appearance of the bands in the range of 1350 to 1450 cm^{-1} was attributed to C–H bending vibration from the methylene groups. Finally, there

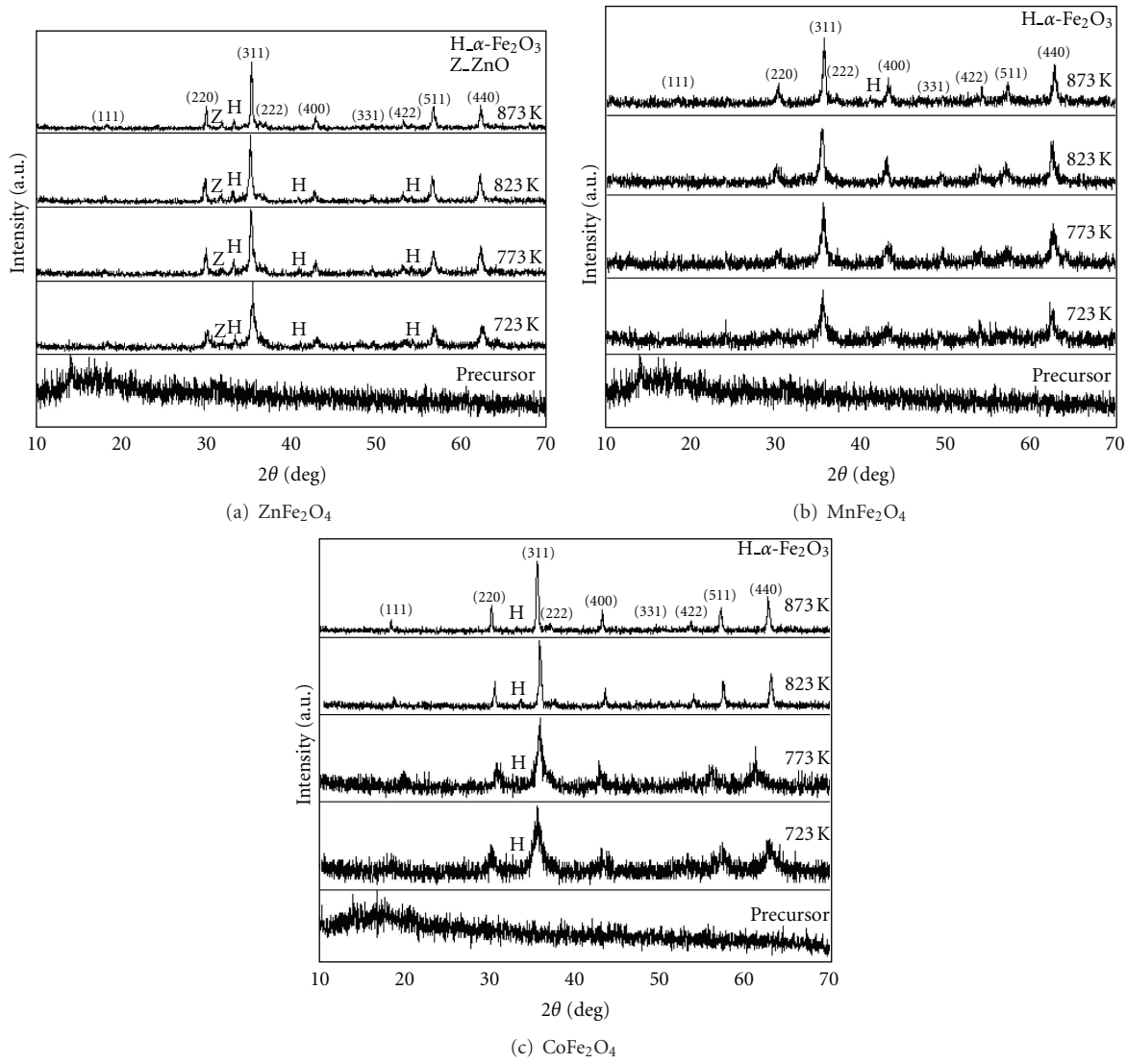

Figure 2: XRD patterns of precursors and metal ferrite nanoparticles of (a) $ZnFe_2O_4$, (b) $MnFe_2O_4$, and (c) $CoFe_2O_4$ calcined at 723, 773, 823, and 873 K.

Table 1: Summery of variation of particle sizes, lattice parameters, saturation magnetization, and coercivity field with temperature calcinations for metal ferrite nanoparticles calcined at 723, 773, 823, and 873 K.

Specimens $MeFe_2O_4$	Calcination temperature (K)	Average particle size XRD (nm)	Average particle size TEM (nm)	Lattice parameter (nm)	Saturation magnetization M_s (emu/g)	Coercivity field H_c (Oe)
ZnFerrite 1	723	21	17 ± 7	0.8498	4.49	Negligible
ZnFerrite 2	773	24	22 ± 2.5	0.8468	2.66	Negligible
ZnFerrite 3	823	31	27 ± 5	0.8471	1.81	Negligible
ZnFerrite 4	873	33	31 ± 11	0.8479	0.74	Negligible
MnFerrite 1	723	15	12 ± 4	0.8524	3.06	Negligible
MnFerrite 2	773	17	15 ± 2	0.8577	6.31	Negligible
MnFerrite 3	823	20	17 ± 5	0.8558	7.96	Negligible
MnFerrite 4	873	23	22 ± 4	0.8537	15.78	Negligible
CoFerrite 1	723	15.5	14 ± 8	0.8356	2.14	823
CoFerrite 2	773	16.5	17 ± 6	0.8348	9.84	1225
CoFerrite 3	823	34	29 ± 9	0.8375	18.02	1791
CoFerrite 4	873	37	34 ± 5	0.8368	23.47	1163

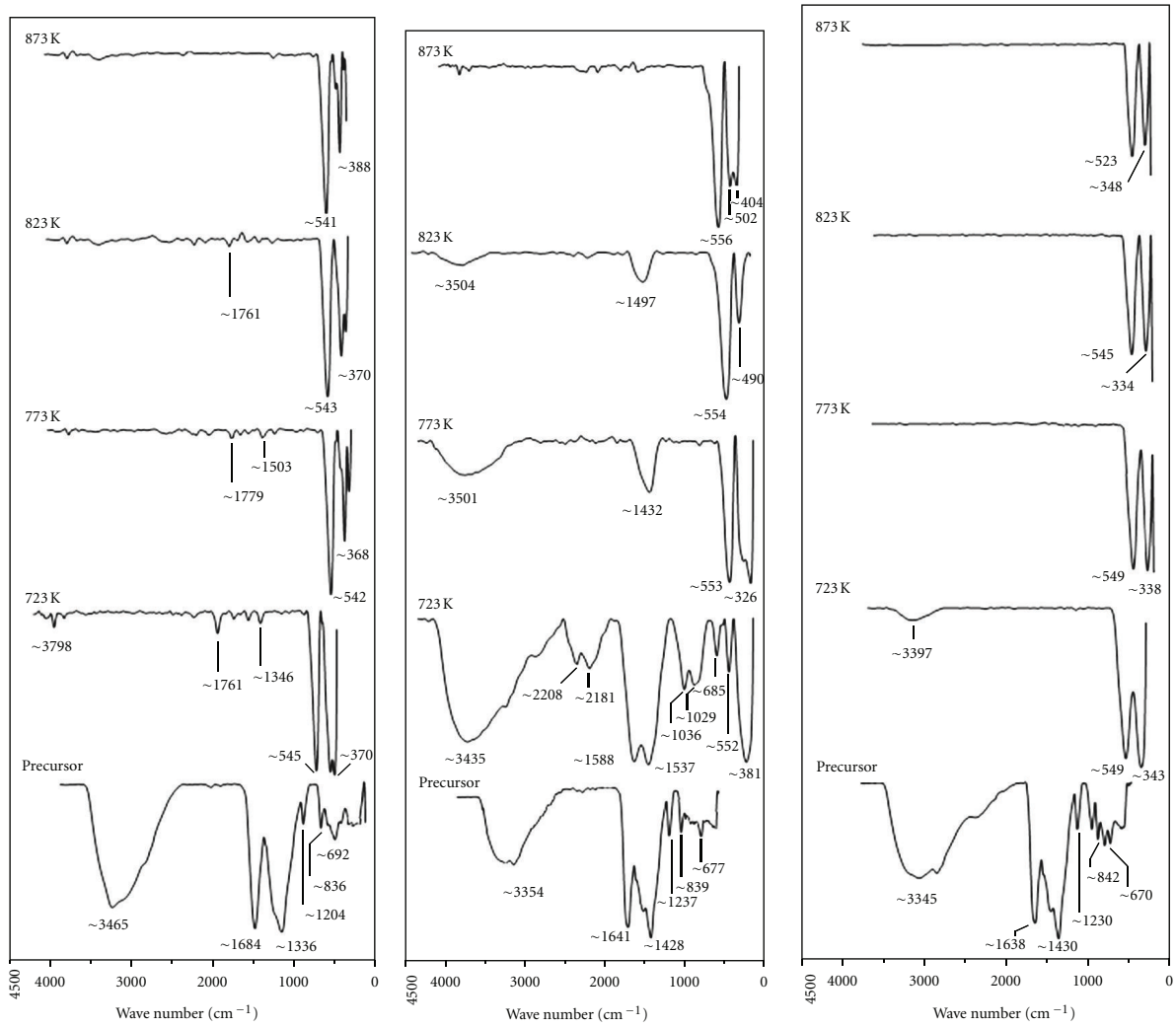

FIGURE 3: FT-IR spectra of precursors and metal ferrite nanoparticles of (a) $ZnFe_2O_4$, (b) $MnFe_2O_4$, and (c) $CoFe_2O_4$ calcined at 723, 773, 823, and 873 K.

were bands in the region 1600 to 1800 cm^{-1} and around 3400 to 3500 cm^{-1}, which were associated with C=O stretching vibration and N–H or O–H stretching vibration, respectively [24]. The vibrational spectra of the absorption bands of pure $ZnFe_2O_4$ and $MnFe_2O_4$ nanoparticles were observed at 388 and 541 cm^{-1}, and at 404, 502, and 556 cm^{-1} for the samples calcined at 873 K (shown in Figures 3(a) and 3(b)). In these two ferrite nanoparticles, at the lower temperature of 873 K, however, there were still traces of broadband absorption peaks at 1497, 1761, and 3504 cm^{-1} due to traces of adsorbed or atmospheric CO_2 and O–H stretching vibration, respectively, while, in $CoFe_2O_4$ nanoparticles (Figure 3(c)), at the lower temperature of 773 K, there was still a trace of a broadband absorption peaks at 3397 cm^{-1} due to ester formation as consequence of the scission of the O–H stretching vibration (Figure 3(c) at 723 K). This suggests that, in thermal treatment method, the calcination temperature of pure cobalt ferrite nanoparticles is lower than pure zinc and manganese ferrite nanoparticles [25–27]. This IR analysis was very useful for establishing the calcination temperature because it removed unwanted ions that may pollute the crystal lattice during preparation.

The TEM images (Figures 4, 5, and 6) show the size, shape, and distribution of $ZnFe_2O_4$, $MnFe_2O_4$, and $CoFe_2O_4$ nanoparticles at different calcination temperatures from 723 to 873 K. The results indicate that the samples prepared by the thermal treatment method were uniform in morphology and particle size distribution. The average particle size of the $ZnFe_2O_4$, $MnFe_2O_4$, and $CoFe_2O_4$ nanoparticles were determined by TEM which increased with the calcinations temperature and they had good agreement with XRD results (Table 1). This suggested that several neighboring particles fused together to increase the particle size by the melting of their surfaces [28]. Particle size enlargement due to grain growth has been observed previously in zinc, manganese, and cobalt ferrite systems at higher calcination temperatures [25–27].

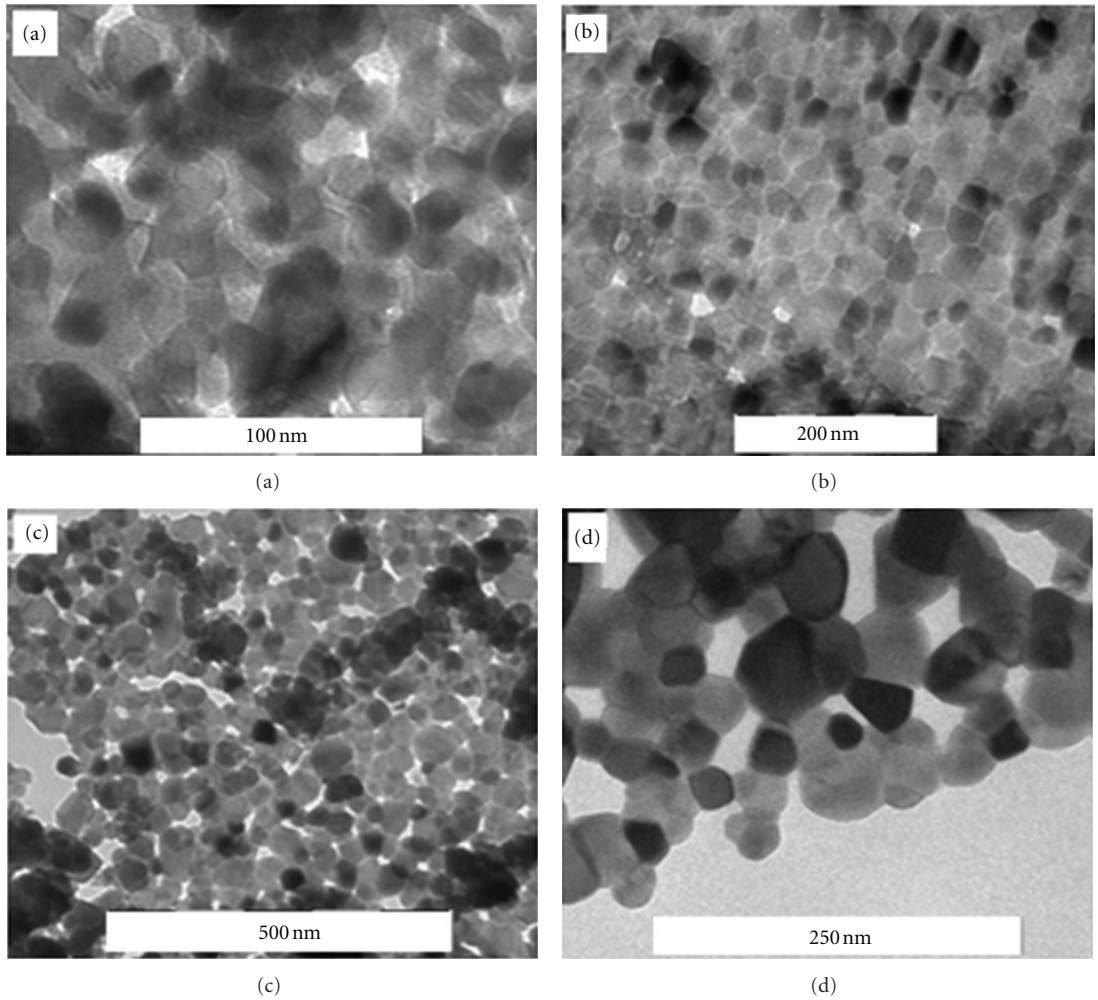

Figure 4: TEM images of zinc ferrite nanoparticles calcined at (a) 723, (b), 773 (c), and 823 (d) 873 K.

3.3. Magnetic Properties of Precursors and MFe_2O_4 Nanoparticles. The room temperature (300 K) magnetic properties of the prepared precursors and MFe_2O_4 nanoparticles calcined at different temperatures were investigated by the VSM technique in the range of approximately −15 to +15 kOe. Except for the precursors which were nonmagnetic material, the calcined samples exhibited different magnetic behaviors. The room temperature magnetic behaviors of metal ferrite nanoparticles which are fabricated by thermal treatment method can be explained as the results of the four important factors: cationic distribution in spinel structure, the heating rate of calcinations, impurity phase of α-Fe_2O_3, and the surface spin structure of nanoparticles. Although all of these factors can be effective in magnetic behaviors, their effects on the ferrite nanoparticles with different structures are not similar.

Figure 7 shows the magnetization curves of precursor and $ZnFe_2O_4$ nanoparticles at (a) 723, (b) 773, (c) 823, and (d) 873 K. Their coercivity fields (H_c) are almost negligible, and all of them exhibit superparamagnetic behaviours. Table 1 provides the values of saturation magnetization (M_s) of the calcined samples, along with calcinations temperatures and particle sizes. These data make it clear that different parameters were responsible for the saturation magnetization decreasing from 4.49 to 0.74 emu/g when the particle size increased from 17 to 31 nm. Cation inversion is one of the most important parameters that can be effective in the variation of the magnetic properties of zinc ferrite nanoparticles from the properties of the bulk form of the same material. In bulk form, zinc ferrite has a normal spinel structure in which all Zn^{2+} ions are in A sites and Fe^{3+} ions are distributed in B sites [29]. However, in bulk, zinc ferrite only occurs in intra-sub-lattice (B-B) exchange interactions, and it does not have intrasublattice (A-A) exchange interactions or intersublattice (A-B) superexchange interactions [30]. Intersublattice (A-B) superexchange interactions of the cations are much stronger than the (A-A) and (B-B) interactions [4]. Due to the cation inversion, which originates from thermal and mechanical treatment [21], the structure of $ZnFe_2O_4$ transfers from a normal spinel structure to a mixed spinel structure [30]. This cation inversion causes the zinc ferrite nanoparticles to experience intersublattice (A-B) superexchange interactions and intrasublattice (A-A) exchange interactions in addition to intrasublattice (B-B) exchange interactions. But, due to the degree of inversion, which is large for smaller size particles, intersublattice (A-B)

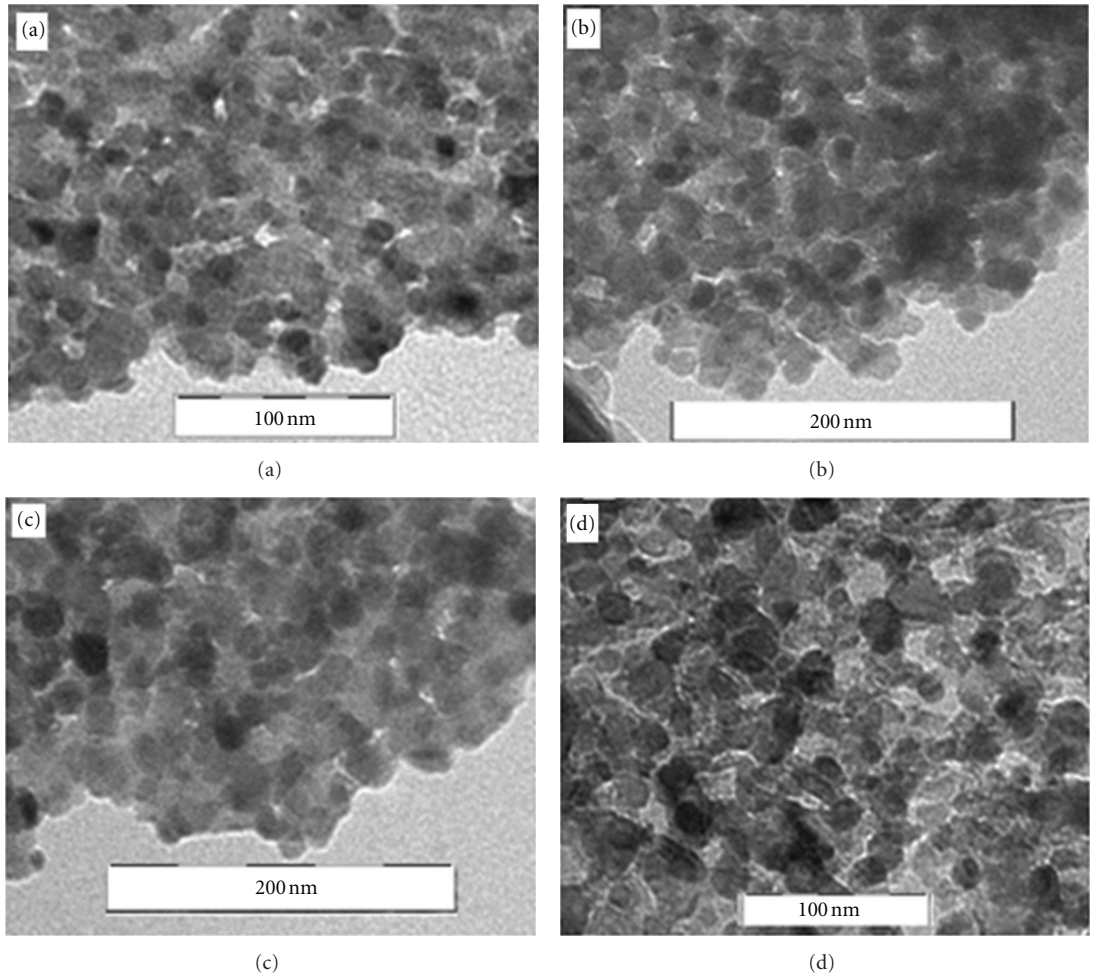

Figure 5: TEM images of manganese ferrite nanoparticles calcined at (a) 723, (b) 773, (c) 823, and (d) 873 K.

super-exchange interactions in smaller size particles occur to a greater extent than in larger size particles. Hence, saturation magnetization increases for smaller size particles [31], using Mossbauer's experiment, showed that the degree of inversion is large in the case of smaller size particles. Also, an impure α-Fe_2O_3 phase was detected by XRD (Figure 2(a)), the heating rate of calcinations and the surface spin structure can be an influence that increases the saturation magnetization in smaller size particles [18].

Figure 8 shows the curves of magnetization of precursor and $MnFe_2O_4$ nanoparticles which exhibited a typical superparamagnetic behavior. Table 1 depicts the values of saturation magnetization (M_s) of different samples. When the calcination temperature increased from 723 K to 873 K, the saturation magnetization increased from 3.06 to 15.78 emu/g. This can be attributed to spin canting and surface spin disorder that occurred in these nanoparticles [32]. The interactions between the A and B sublattices in the spinel lattice system (AB_2O_4) consist of intersublattice (A-B) super-exchange interactions and intrasublattice (A-A) and (B-B) exchange interactions. Intersublattice superexchange interactions of the cations on the (A-B) are much stronger than the (A-A) and (B-B) intrasublattice exchange interactions [4, 33]. As discussed earlier (Figure 2(b)), by increasing the calcination temperature of the $MnFe_2O_4$ nanoparticles, Fe^{3+} ions transferred from B site to A site, so, consequently, the accumulation of Fe^{3+} ions increased in A site; however, the $Fe_A{}^{3+}$-$Fe_B{}^{3+}$ superexchange interactions increased ($Fe_A{}^{3+}$-$Fe_B{}^{3+}$ interactions were twice as strong as the $Mn_A{}^{2+}$-$Fe_B{}^{3+}$ interactions), and this can lead to an increase in saturation magnetization in $MnFe_2O_4$ nanoparticles [34]. Aslibeiki et al. [35] showed that saturation magnetization increases with increasing temperature and particle size in $MnFe_2O_4$ nanoparticles.It has been reported [36] that the spin disorder may occur on the surface of the nanoparticles as well as within the cores of the nanoparticles due to vacant sublattice disorder sites ($Fe_A{}^{3+}$) and poor crystal structure. The other point that is understood from Table 1 is that the values of saturation magnetization are expressively lower than those reported for the bulk $MnFe_2O_4$ (80 emu/g) [37]. The decrease in saturation magnetization of all the samples compared to that of the bulk is ascribed to the surface effects in these nanoparticles. The existence of an inactive magnetic layer or a disordered layer on the surfaces of the nanoparticles and the heating rate of calcinations can be due to the decrease of saturation magnetization compared to the bulk value [38, 39].

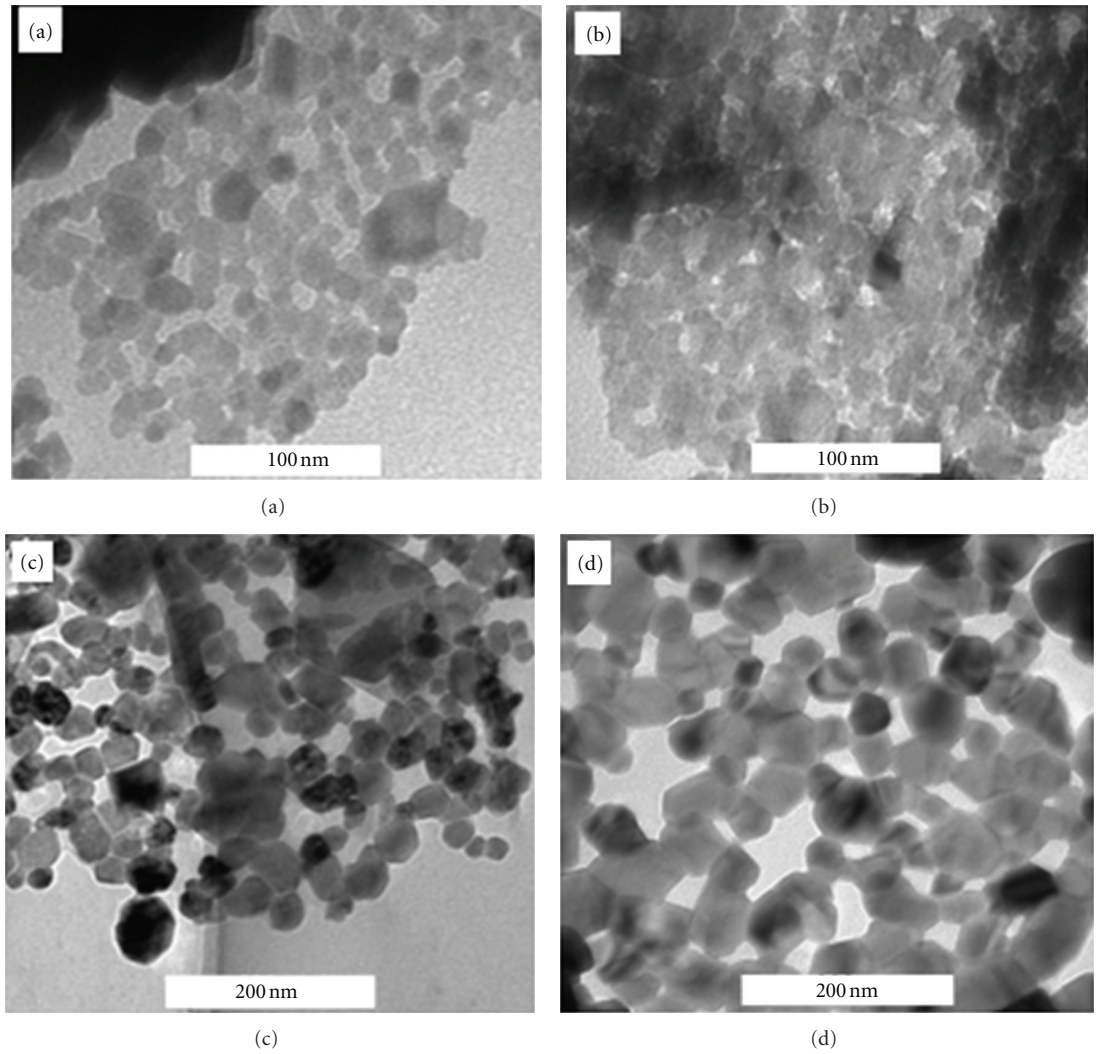

Figure 6: TEM images of cobalt ferrite nanoparticles calcined at (a) 723, (b) 773, (c) 823, and (d) 873 K.

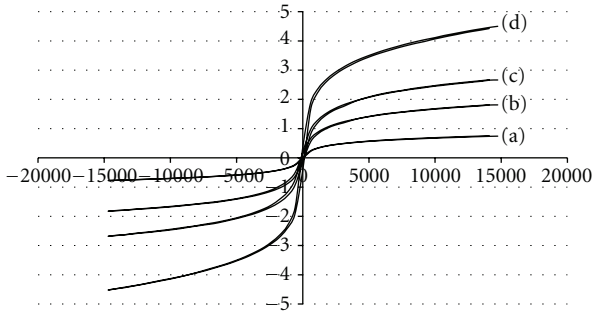

Figure 7: Magnetization curves at room temperature for precursor and zinc ferrite nanoparticles calcined at (a) 723, (b) 773, (c) 823, and (d) 873 K.

Figure 9 shows the M (H) loops of precursor and $CoFe_2O_4$ nanoparticles that were measured at room temperature. Except for the precursor, which was a nonmagnetic material, the calcined samples exhibited typical ferromagnetic behaviors. It is evident in Table 1 that, when the calcinations temperature increases from 723 to 873 K, the saturation magnetization increases from 2.14 to 23.47 emu/g at room temperature. The largest saturation magnetization was 23.47 emu/g for the sample calcined at 873 K, which is much lower than that reported for the multidomain, bulk cobalt ferrite (74.08 emu/g) [40]. The decrease in saturation magnetization of these samples, compared to that of bulk material, depends on different parameters. The decrease in saturation magnetization of these samples, compared to that of bulk material, depends on four factors explained in Section 3.3. It seems that, in inversed spinel ferrite nanoparticles such as cobalt ferrite or nickel ferrite nanoparticles which fabricated by thermal treatment method, the heating rate of calcination is more important than other parameters that can effectively increase or decrease the saturation magnetization [25, 41]. In our experiments, the heating rate of calcination was 10 K/min for cobalt, zinc, and manganese ferrite nanoparticles calcined at 723, 773, 823, and 873 K, which was a medium heating rate. Therefore, it is possible that calcination at a slower heating rate would allow crystallization to be more complete and the magnetic phase could also increase, resulting in larger saturation

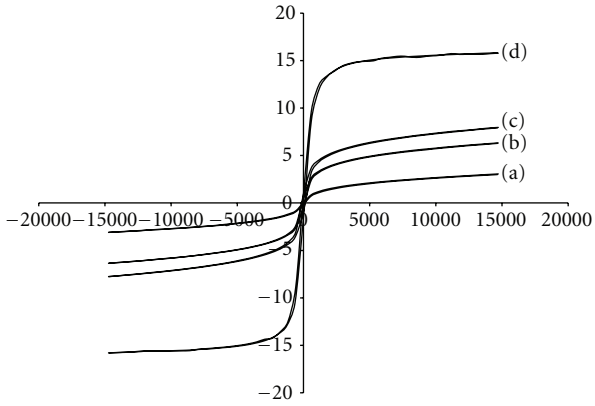

Figure 8: Magnetization curves at room temperature for precursor and manganese ferrite nanoparticles calcined at (a) 723, (b) 773, (c) 823, and (d) 873 K.

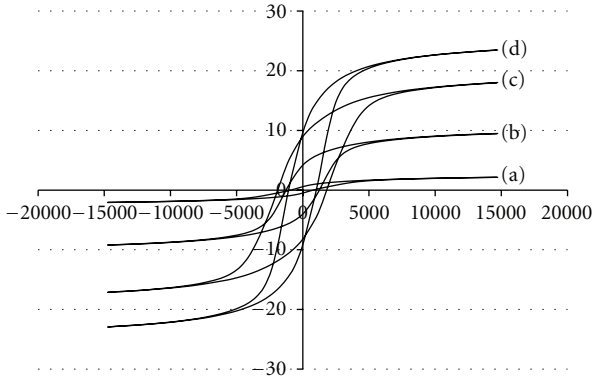

Figure 9: Magnetization curves at room temperature for precursor and cobalt ferrite nanoparticles calcined at (a) 723, (b) 773, (c) 823, and (d) 873 K.

magnetization. Sangmanee and Maensiri [42] showed that saturation magnetization increases from 9.7 to 56.5 emu/g with decreasing the heating rate of calcination from 20 K/min to 5 K/min in cobalt ferrite nanostructures calcined at 773 K and fabricated by electrospinning. In addition, the appearance of the weakly magnetic, impure phase of α-Fe_2O_3 (shown in Figure 2(c)) can reduce the saturation magnetization [18]. Also, the cation site occupancy in $CoFe_2O_4$ nanoparticles is different than in the bulk [43]. In fact, since the nanoparticles are the mixed spinel structure type rather than the inverse spinel structure type (bulk) because of the presence of Co^{3+} ions and also a cation distribution with cobalt ions on the tetrahedral site [44], the saturation magnetization is reduced [45]. In addition, the appearance of the weakly magnetic, impure phase of hematite (shown in Figure 2(c)) can reduce the saturation magnetization [18, 46]. The variations of saturation magnetization and coercivity field with particle size and calcination temperature for cobalt ferrite nanoparticles are listed in Table 1. The saturation magnetization of the calcined samples increases with increasing particle size, which may be attributed to the surface effects in these nanoparticles. The surface of the nanoparticles seems to be composed of some distorted or slanted spins that repel the core spins to align the field direction, consequently, the saturation magnetization increase for larger sizes and decrease for smaller sizes [47]. But the values of the coercivity field have no similar relationship with saturation magnetization, because, when the particle size increases from 14 to 34 nm, the coercivity field increases to 1791 Oe for 29 nm particle size then decreases to 1163 Oe for 34 nm particle size at room temperature. This variation in the value of the coercivity field with particle size can be explained on the basis of domain structure, critical size, and the anisotropy of the crystal [48, 49].

4. Conclusion

The results of this investigation indicate that the thermal treatment method can be used for synthesizing $ZnFe_2O_4$, $MnFe_2O_4$, and $CoFe_2O_4$ nanoparticles using poly(vinyl pyrrolidone) as a capping agent to stabilize the particles and prevent them from agglomerating. XRD patterns and TEM images show the formation of MFe_2O_4 nanoparticles with particle sizes of 17–31 nm, 12–22 nm, and 14–34 nm for $ZnFe_2O_4$, $MnFe_2O_4$, and $CoFe_2O_4$ nanoparticles, respectively. FT-IR confirmed the presence of metal oxide bands at all temperatures and the absence of organic bands at 873 K for zinc and manganese ferrite nanoparticles and at 773 K for the cobalt ferrite nanoparticles. VSM results demonstrated that zinc and manganese ferrite nanoparticles displayed superparamagnetic behaviors while cobalt ferrite nanoparticles exhibited ferromagnetic behaviors.

Acknowledgments

The authors would like to thank Miss Fatemeh Moazami Goodarzi for her great assistance in the chemical mechanism study. This work was supported by the Ministry of Higher Education of Malaysia under the FRGS Grant and Universiti Putra Malaysia under the RUGS Grant.

References

[1] G. Maggioni, A. Vomiero, S. Carturan et al., "Structure and optical properties of Au-polyimide nanocomposite films prepared by ion implantation," *Applied Physics Letters*, vol. 85, no. 23, pp. 5712–5714, 2004.

[2] K. A. Bogle, S. D. Dhole, and V. N. Bhoraskar, "Silver nanoparticles: synthesis and size control by electron irradiation," *Nanotechnology*, vol. 17, no. 13, pp. 3204–3208, 2006.

[3] P. Gangopadhyay, R. Kesavmoorthy, S. Bera et al., "Preferential facet of nanocrystalline silver embedded in polyethylene oxide nanocomposite and its antibiotic behaviors," *Physical Review Letters*, vol. 94, pp. 47403–47404, 2005.

[4] M. Atif, S. K. Hasanain, and M. Nadeem, "Magnetization of sol-gel prepared zinc ferrite nanoparticles: effects of inversion and particle size," *Solid State Communications*, vol. 138, no. 8, pp. 416–421, 2006.

[5] J. Z. Jiang, P. Wynn, S. Mørup, T. Okada, and F. J. Berry, "Magnetic structure evolution in mechanically milled nanostructured $ZnFe_2O_4$ particles," *Nanostructured Materials*, vol. 12, no. 5, pp. 737–740, 1999.

[6] S. D. Shenoy, P. A. Joy, and M. R. Anantharaman, "Effect of mechanical milling on the structural, magnetic and dielectric properties of coprecipitated ultrafine zinc ferrite," *Journal of Magnetism and Magnetic Materials*, vol. 269, no. 2, pp. 217–226, 2004.

[7] D. E. Zhang, X. J. Zhang, X. M. Ni, H. G. Zhang, and D. D. Yang, "Design and experiment of the self-propelled combine harvester for corn and stalk," *Journal of Magnetism and Magnetic Materials*, vol. 292, pp. 79–82, 2005.

[8] H. Li, H. Z. Wu, and G. X. Xiao, "Effects of synthetic conditions on particle size and magnetic properties of $NiFe_2O_4$," *Powder Technology*, vol. 198, no. 1, pp. 157–166, 2010.

[9] A. Kale, S. Gubbala, and R. D. K. Misra, "Magnetic behavior of nanocrystalline nickel ferrite synthesized by the reverse micelle technique," *Journal of Magnetism and Magnetic Materials*, vol. 277, no. 3, pp. 350–358, 2004.

[10] J. F. Hochepied, P. Bonville, and M. P. Pileni, "Nonstoichiometric zinc ferrite nanocrystals: syntheses and unusual magnetic properties," *Journal of Physical Chemistry B*, vol. 104, no. 5, pp. 905–912, 2000.

[11] P. Sivakumar, R. Ramesh, A. Ramanand, S. Ponnusamy, and C. Muthamizhchelvan, "Synthesis and characterization of $NiFe_2O_4$ nanosheet via polymer assisted co-precipitation method," *Materials Letters*, vol. 65, no. 3, pp. 483–485, 2011.

[12] M. M. Koebel, L. C. Jones, and G. A. Somorjai, "Preparation of size-tunable, highly monodisperse PVP-protected Pt-nanoparticles by seed-mediated growth," *Journal of Nanoparticle Research*, vol. 10, no. 6, pp. 1063–1069, 2008.

[13] A. R. Roosen and W. C. Carter, "Simulations of microstructural evolution: anisotropic growth and coarsening," *Physica A*, vol. 261, no. 1-2, pp. 232–247, 1998.

[14] G. Ghosh, M. Kanti Naskar, A. Patra, and M. Chatterjee, "Synthesis and characterization of PVP-encapsulated ZnS nanoparticles," *Optical Materials*, vol. 28, no. 8-9, pp. 1047–1053, 2006.

[15] H. Shao, Y. Huang, H. Lee, Y. J. Suh, and C. O. Kim, "Effect of PVP on the morphology of cobalt nanoparticles prepared by thermal decomposition of cobalt acetate," *Current Applied Physics*, vol. 6, no. 1, pp. e195–e197, 2006.

[16] W. Y. Huang and G. C. Xu, "Characterization of nano-Ag/PVP composites synthesized via ultra-violet irradiation," *Journal of Coal Science and Engineering*, vol. 16, no. 2, pp. 188–192, 2010.

[17] M. Tsuji, M. Hashimoto, Y. Nishizawa, and T. Tsuji, "Synthesis of gold nanorods and nanowires by a microwave-polyol method," *Materials Letters*, vol. 58, no. 17-18, pp. 2326–2330, 2004.

[18] P. Laokul, V. Amornkitbamrung, S. Seraphin, and S. Maensiri, "Characterization and magnetic properties of nanocrystalline $CuFe_2O_4$, $NiFe_2O_4$, $ZnFe_2O_4$ powders prepared by the Aloe vera extract solution," *Current Applied Physics*, vol. 11, no. 1, pp. 101–108, 2011.

[19] L. Zhen, K. He, C. Y. Xu, and W. Z. Shao, "Synthesis and characterization of single-crystalline $MnFe_2O_4$ nanorods via a surfactant-free hydrothermal route," *Journal of Magnetism and Magnetic Materials*, vol. 320, no. 21, pp. 2672–2675, 2008.

[20] J. Jiang and L. H. Ai, "Synthesis and characterization of Fe-Co binary ferrospinel nanospheres via one-step nonaqueous solution pathway," *Materials Letters*, vol. 64, no. 8, pp. 945–947, 2010.

[21] J. P. Singh, R. C. Srivastava, H. M. Agrawal, and R. Kumar, "Magnetic behaviour of nanosized zinc ferrite under heavy ion irradiation," *Nuclear Instruments and Methods in Physics Research B*, vol. 268, no. 9, pp. 1422–1426, 2010.

[22] B. D. Cullity, *Elements of X-ray Diffraction*, Addison-Wesley, London, UK, 2nd edition, 1978.

[23] R. K. Selvan, C. O. Augustin, L. J. Berchmans, and R. Saraswathi, "Combustion synthesis of $CuFe_2O_4$," *Materials Research Bulletin*, vol. 38, no. 1, pp. 41–54, 2003.

[24] M. I. Loría-Bastarrachea, W. Herrera-Kao, J. V. Cauich-Rodríguez, J. M. Cervantes-Uc, H. Vázquez-Torres, and A. Ávila-Ortega, "A TG/FTIR study on the thermal degradation of poly(vinyl pyrrolidone)," *Journal of Thermal Analysis and Calorimetry*, vol. 104, no. 2, pp. 737–742, 2011.

[25] M. G. Naseri, E. B. Saion, H. Abbastabar Ahangar, A. H. Shaari, and M. Hashim, "Simple synthesis and characterization of cobalt ferrite nanoparticles by a thermal treatment method," *Journal of Nanomaterials*, vol. 2010, Article ID 907686, 8 pages, 2010.

[26] M. G. Naseri, E. B. Saion, H. A. Ahangar, M. Hashim, and A. H. Shaari, "Synthesis and characterization of manganese ferrite nanoparticles by thermal treatment method," *Journal of Magnetism and Magnetic Materials*, vol. 323, no. 13, pp. 1745–1749, 2011.

[27] M. G. Naseri, E. B. Saion, M. Hashim, A. H. Shaari, and H. A. Ahangar, "Synthesis and characterization of zinc ferrite nanoparticles by a thermal treatment method," *Solid State Communications*, vol. 151, no. 14-15, pp. 1031–1035, 2011.

[28] Y. Qu, H. Yang, N. Yang, Y. Fan, H. Zhu, and G. Zou, "The effect of reaction temperature on the particle size, structure and magnetic properties of coprecipitated $CoFe_2O_4$ nanoparticles," *Materials Letters*, vol. 60, no. 29-30, pp. 3548–3552, 2006.

[29] D. S. Mathew and R. S. Juang, "An overview of the structure and magnetism of spinel ferrite nanoparticles and their synthesis in microemulsions," *Chemical Engineering Journal*, vol. 129, no. 1–3, pp. 51–65, 2007.

[30] F. S. Li, L. Wang, J. B. Wang et al., "Site preference of Fe in nanoparticles of $ZnFe_2O_4$," *Journal of Magnetism and Magnetic Materials*, vol. 268, no. 3, pp. 332–339, 2004.

[31] M. K. Roy, B. Haldar, and H. C. Verma, "Characteristic length scales of nanosize zinc ferrite," *Nanotechnology*, vol. 17, no. 1, pp. 232–237, 2006.

[32] Z. Gu, X. Xiang, G. Fan, and F. Li, "Facile synthesis and characterization of cobalt ferrite nanocrystals via a simple reduction-oxidation route," *Journal of Physical Chemistry C*, vol. 112, no. 47, pp. 18459–18466, 2008.

[33] S. Ammar, N. Jouini, F. Fiévet et al., "Magnetic properties of zinc ferrite nanoparticles synthesized by hydrolysis in a polyol medium," *Journal of Physics Condensed Matter*, vol. 18, no. 39, pp. 9055–9069, 2006.

[34] J. Li, H. Yuan, G. Li, Y. Liu, and J. Leng, "Cation distribution dependence of magnetic properties of solgel prepared $MnFe_2O_4$ spinel ferrite nanoparticles," *Journal of Magnetism and Magnetic Materials*, vol. 322, no. 21, pp. 3396–3400, 2010.

[35] B. Aslibeiki, P. Kameli, H. Salamati, M. Eshraghi, and T. Tahmasebi, "Superspin glass state in $MnFe_2O_4$ nanoparticles," *Journal of Magnetism and Magnetic Materials*, vol. 322, no. 19, pp. 2929–2934, 2010.

[36] M. P. Morales, S. Veintemillas-Verdaguer, M. I. Montero et al., "Surface and internal spin canting in γ-Fe_2O_3 nanoparticles," *Chemistry of Materials*, vol. 11, no. 11, pp. 3058–3064, 1999.

[37] V. A. M. Brabers, "Progress in spinel ferrite research," in *Handbook of Magnetic Materials*, K. H. J. Buschow, Ed., vol. 8, chapter 3, pp. 189–324, Elsevier, New York, NY, USA, 1995.

[38] J. Nogués, J. Sort, V. Langlais et al., "Exchange bias in nanostructures," *Physics Reports*, vol. 422, no. 3, pp. 65–117, 2005.

[39] K. Maaz, A. Mumtaz, S. K. Hasanain, and A. Ceylan, "Synthesis and magnetic properties of cobalt ferrite ($CoFe_2O_4$) nanoparticles prepared by wet chemical route," *Journal of Magnetism and Magnetic Materials*, vol. 308, no. 2, pp. 289–295, 2007.

[40] M. P. Gonzalez-Sandoval, A. M. Beesley, M. Miki-Yoshida, L. Fuentes-Cobas, and J. A. Matutes-Aquino, "Comparative study of the microstructural and magnetic properties of spinel ferrites obtained by co-precipitation," *Journal of Alloys and Compounds*, vol. 369, no. 1-2, pp. 190–194, 2004.

[41] M. G. Naseri, E. B. Saion, H. A. Ahangar, M. Hashim, and A. H. Shaari, "Simple preparation and characterization of nickel ferrite nanocrystals by a thermal treatment method," *Powder Technology*, vol. 212, no. 1, pp. 80–88, 2011.

[42] M. Sangmanee and S. Maensiri, "Nanostructures and magnetic properties of cobalt ferrite ($CoFe_2O_4$) fabricated by electrospinning," *Applied Physics A*, vol. 97, no. 1, pp. 167–177, 2009.

[43] F. Nakagomi, S. W. Da Silva, V. K. Garg et al., "The influence of cobalt population on the structural properties of CoxFe3-x O4," *Journal of Applied Physics*, vol. 101, no. 9, Article ID 09M514, pp. 09M514–09M517, 2007.

[44] E. V. Gopalan, I. A. Al-Omari, D. S. Kumar, Y. Yoshida, P. A. Joy, and M. R. Anantharaman, "Inverse magnetocaloric effect in sol-gel derived nanosized cobalt ferrite," *Applied Physics A*, vol. 99, no. 2, pp. 497–503, 2010.

[45] A. Franco Jr and F. C. E Silva, "High temperature magnetic properties of cobalt ferrite nanoparticles," *Applied Physics Letters*, vol. 96, no. 17, Article ID 172505, pp. 172505–172508, 2010.

[46] Y. Kinemuchi, K. Ishizaka, H. Suematsu, W. Jiang, and K. Yatsui, "Magnetic properties of nanosize $NiFe_2O_4$ particles synthesized by pulsed wire discharge," *Thin Solid Films*, vol. 407, no. 1-2, pp. 109–113, 2002.

[47] R. H. Kodama, A. E. Berkowitz, E. J. McNiff Jr, and S. Foner, "Surface spin disorder in ferrite nanoparticles," *Journal of Applied Physics*, vol. 81, no. 8, pp. 5552–5557, 1997.

[48] M. V. Vasic, B. Antic, A. Kremenović et al., "Zn,Ni ferrite/NiO nanocomposite powder obtained from acetylacetonato complexes," *Nanotechnology*, vol. 17, no. 19, pp. 4877–4884, 2006.

[49] B. D. Cullity, *Introduction to Magnetic Materials*, Addison-Wesley, London, UK, 1972.